

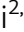










PWWP2B promotes DNA end resection and homologous recombination

Min Kyung Ju^{1,†} , Joo Rak Lee^{1,†} , Yeonsong Choi^{2,†} , Seon Young Park^{3,†} , Hee Jung Sul^{4,†}, Hee Jin Chung¹, Soyeong An¹, Semin Lee², Eunyoung Jung³, Bohyun Kim⁴, Bo Youn Choi⁴ , Bum Jun Kim⁵, Hyeong Su Kim⁵ , Hyun Lim⁵, Ho Suk Kang⁵, Jae Seung Soh⁵, Kyungjae Myung^{1,6} , Kab Choong Kim⁷, Ji Woong Cho⁷, Jinwon Seo⁸, Tae Moon Kim⁶ , Ja Yil Lee^{1,6}, Yonghwan Kim^{3,*} , Hongtae Kim^{1,6,**}  & Dae Young Zang^{4,5,***} 

Abstract

Genome instability is one of the leading causes of gastric cancers. However, the mutational landscape of driver genes in gastric cancer is poorly understood. Here, we investigate somatic mutations in 25 Korean gastric adenocarcinoma patients using whole-exome sequencing and show that *PWWP2B* is one of the most frequently mutated genes. *PWWP2B* mutation correlates with lower cancer patient survival. We find that *PWWP2B* has a role in DNA double-strand break repair. As a nuclear protein, *PWWP2B* moves to sites of DNA damage through its interaction with UHRF1. Depletion of *PWWP2B* enhances cellular sensitivity to ionizing radiation (IR) and impairs IR-induced foci formation of RAD51. *PWWP2B* interacts with MRE11 and participates in homologous recombination via promoting DNA end-resection. Taken together, our data show that *PWWP2B* facilitates the recruitment of DNA repair machinery to sites of DNA damage and promotes HR-mediated DNA double-strand break repair. Impaired *PWWP2B* function might thus cause genome instability and promote gastric cancer development.

Keywords end resection; gastric cancer; homologous recombination; PWWP2B; UHRF1

Subject Categories Cancer; DNA Replication, Recombination & Repair

DOI 10.15252/embr.202153492 | Received 22 June 2021 | Revised 18 April 2022 | Accepted 2 May 2022 | Published online 18 May 2022

EMBO Reports (2022) 23: e53492

Introduction

Gastric cancer is the fifth most common cancer in the world, and the third leading cause of cancer-related death globally (Fitzmaurice *et al*, 2017). Most gastric cancer is adenocarcinoma, and environmental and genetic factors contribute to the development of the disease. Depending upon the location of gastric cancer, *Helicobacter pylori* infection, smoking, high salt intake, obesity, and gastroesophageal reflux are known as risk factors for gastric cancer (Karimi *et al*, 2014). However, mounting evidence suggests that genetic instability also contributes to the onset of gastric tumorigenesis. Two types of genomic instabilities are generally recognized in gastric cancers, microsatellite instability (MSI), and chromosomal instability. Both genetic changes are not necessarily independent and may overlap in some cases (Hiyama *et al*, 2004; Cancer Genome Atlas Research Network, 2014). A high degree of MSI (5–50%) has been identified in a range of gastric cancer with significant differences between ethnic groups. MSI mostly attributes to the inactivation of genes, particularly *MLH1* or *MSH2*, which are important in the mismatch repair (MMR) pathway (Falchetti *et al*, 2008; Haron *et al*, 2019). Mismatch repair defects cause the accumulation of mutations in the coding or non-coding regions. As clinical outcomes of gastric cancers vary according to the status of genetic changes, establishing defined molecular classifications of gastric cancers is urgently needed. However, such genetic or epigenetic changes leading to the initiation and/or progression of both types of gastric cancers remain largely unknown.

Genetic materials are constitutively challenged by a variety of intrinsic or extrinsic insults, and the resulting genetic lesions unless

1 Department of Biological Sciences, Ulsan National Institute of Science and Technology, Ulsan, Korea

2 Department of Biomedical Engineering, Ulsan National Institute of Science and Technology, Ulsan, Korea

3 Department of Biological Sciences, Research Institute of Women's Health, Sookmyung Women's University, Seoul, Korea

4 Hallym Translational Research Institute, Hallym University Sacred Heart Hospital, Anyang-si, Korea

5 Department of Internal Medicine, Hallym University Sacred Heart Hospital, Hallym University College of Medicine, Anyang-si, Korea

6 Center for Genomic Integrity Institute for Basic Science (IBS), Ulsan, Korea

7 Department of Surgery, Hallym University Medical Center, Hallym University College of Medicine, Anyang-si, Korea

8 Department of Pathology, Hallym University Sacred Heart Hospital, Hallym University College of Medicine, Anyang-si, Korea

*Corresponding author. Tel: +82 2 710 9552; Fax: +82 2 2077 7322; E-mail: yhkim@sookmyung.ac.kr

**Corresponding author. Tel: +82 52 217 5404; Fax: +82 52 217 7015; E-mail: khtcat@unist.ac.kr

***Corresponding author. Tel: +82 31 380 3704; Fax: +82 31 386 1528; E-mail: fhdzang@hallym.or.kr

[†]These authors contributed equally to this work

repaired properly lead to the impairment of gene function, the loss of cellular homeostasis, genome instability, and, eventually, tumorigenesis (Mills *et al*, 2003; Lee *et al*, 2016). Therefore, cells have evolved efficient DNA damage response (DDR) and DNA repair pathways for genome maintenance. Among the types of DNA damage, DNA double-strand breaks (DSBs) are a deadly type of DNA damage as they can lead to the physical dissociation of chromosomes (Aparicio *et al*, 2014). There are two major pathways for repairing DSBs, homologous recombination (HR) and non-homologous end-joining (NHEJ). However, the underlying molecular mechanism for the pathway choice of DSB repair is not yet fully understood. An E3 ubiquitin ligase, ubiquitin-like with PHD and RING finger domains1 (UHRF1), also known as Np95 and ICBP90, was reported as one of the key factors regulating the pathway choice of DSB repair, especially channeling repair into the HR pathway in the S/G2 phases of the cell cycle. RIF1 was shown to accumulate at DSB sites in the G1 phase to inhibit BRCA1-dependent HR. Phosphorylated UHRF1 was recruited to the sites of DNA damage through its direct interaction with BRCA1 and then catalyzed the K63-linked ubiquitination of RIF1. It was proposed that the ubiquitination of RIF1 leads to the loss of its association with 53BP1 at the DSB sites, which in turn, promoted HR during the S/G2 phases (Zhang *et al*, 2016). During HR, the MRE11-RAD50-NBS1 (MRN) complex first recognizes DSBs and then initiates DNA end resection that generates 3' single-stranded DNA (ssDNA) overhangs. The emergent ssDNA is rapidly bound by the RPA complex, which is subsequently displaced by RAD51 recombinase. RAD51 loads onto ssDNA and forms a RAD51-ssDNA nucleoprotein filament, enabling homology search and strand invasion (Scully *et al*, 2019). For DNA end resection, CtIP was shown to localize to the sites of DSBs and associate with the MRN complex. CtIP at DSB sites facilitates DNA end resection by promoting the nuclease activity of the MRN complex. This process is regarded as a key step in HR-mediated repair (Sartori *et al*, 2007). It was shown UHRF1 was sufficient to channel repair to the HR pathway in the S phase, whereas both UHRF1 and CtIP were required for this process in the G2 phase (Zhang *et al*, 2016). However, the exact molecular basis for UHRF1 regulation at the sites of DSBs is not fully understood.

The PWWP domain is one of the Royal superfamily protein domains. The PWWP domain is named after a conserved Pro-Trp-Trp-Pro motif, although only the last Pro is unconditionally conserved. Twenty proteins have been identified that harbor the PWWP domain in humans (Maurer-Stroh *et al*, 2003; Qin & Min, 2014). Those proteins are mostly chromatin-associated and implicated in the regulation of gene expression and/or DNA repair pathways. Structural analysis of the PWWP domain demonstrated that prominent positively charged amino acids were located on surfaces, which enabled proteins to be associated with DNA in general (Qiu *et al*, 2002; Eidahl *et al*, 2013). In addition, accumulated evidence has demonstrated that the PWWP domain is responsible for reading the modified modes of chromatin and nucleosomes (Qiu *et al*, 2012; Eidahl *et al*, 2013; van Nuland *et al*, 2013). The function of many PWWP-containing proteins have been characterized, but the molecular and cellular functions of the PWWP2B protein remain largely unknown. Recently, it was reported that the PWWP2B protein along with PWWP2A formed a complex with NuRD subunits such as MTA1/2/3, HDAC1/2, and RBBP4/7 and played important roles in the regulation of histone acetylation and gene expression (Zhang

et al, 2018). However, the other functional roles of PWWP2B protein in DNA repair have not yet been determined.

In this study, through the whole-exome sequencing (WES) analysis of 25 Korean gastric adenocarcinoma patient samples, we identified the *PWWP2B* gene as one of the most frequently mutated genes in these patients. We showed that PWWP2B, a new factor interacting with UHRF1, mobilized to the sites of DNA damage by binding to UHRF1 and that PWWP2B was important for HR-mediated DSB repair. We also showed that the depletion of PWWP2B severely impaired IR-induced BRCA1, RPA2, and RAD51 foci formation hinting that PWWP2B promoted DNA end resection in the process of HR-mediated repair. Notably, the mutation status of PWWP2B strongly correlated with the overall survival of cancer patients. In summary, our findings identified PWWP2B as a new DDR factor that interacted with UHRF1 and promoted HR-mediated DSB repair via facilitating DNA end resection. The findings may be translated into clinical use, including the diagnosis and prognosis of gastric cancer patients.

Results

Recurrent PWWP2B mutations are identified in whole-exome sequencing analysis of stomach adenocarcinoma samples

To identify the genetic alterations causing STAD, we collected genomic DNA from 25 Korean STAD patients' samples. Tumor tissues were collected from 25 gastric cancer patients diagnosed at Hallym University Sacred Heart Hospital from June 2013 to April 2017. At the time of diagnosis, six of 25 patients had metastatic disease and endoscopic biopsies were performed to obtain tissue. The other 19 patients had localized or locally advanced disease at diagnosis (stage I, two patients; stage II or III, 17 patients) and underwent curative surgical resections. Tumor tissues of these patients were obtained from the surgical specimens (Table 1). We performed whole-exome sequencing (WES) to determine somatically altered genes in the genomic DNAs. Thirty-two genes were identified as significantly recurrently mutated genes using the MutSigCV algorithm (Fig) ($-\log(P\text{-value}) > 5$). Some of the significantly mutated genes such as *TP53*, *PHGR1*, *BAX*, *PRRT2*, *OR7E24*, and *CDH24* were previously reported to be associated with stomach cancer (Ouyang *et al*, 1998; Cancer Genome Atlas Research Network, 2014; An *et al*, 2015; Alves *et al*, 2017; Cortes-Ciriano *et al*, 2017). However, there were other genes including *WBPI*, *DAZAPI*, *KIAA1919*, and *PWWP2B* whose functional roles in stomach cancer development are not well known. Specifically, *PWWP2B* was mutated in eight out of 25 samples, which was the second most frequently mutated gene in our dataset, but its molecular mechanism in biological pathways has been rarely addressed. We identified ten mutations in *PWWP2B* (Fig 1B). Among them, only the P86 frame-shift (fs) mutation was detected in more than one sample in our dataset. Seven out of nine (78%) uniquely identified *PWWP2B* mutations were predicted to be either deleterious or having high impact (Appendix Table S1). Furthermore, five *PWWP2B* missense mutation loci were highly conserved (conservation score > 80%) at the protein sequence level with one exception of p.Arg68Trp (conservation score < 50%; Appendix Fig S1). The distribution of *PWWP2B* mutations reported from large-scale genomic studies of TCGA stomach

Table 1. Association between prognostic factors and overall patient survival. Multivariate Cox regression analysis was performed by selecting variables with a P-value of < 0.10 in the univariate analysis.

Variables (n)	OS, months		Univariate analysis		Multivariate analysis	
	Mean ^a	95% CI	HR (95% CI)	P	HR (95% CI)	P
Sex						
Male (18)	39.3	26.2–52.3	Reference		Reference	
Female (7)	60.3	40.7–80.0	0.45 (0.10–2.08)	0.31	–	–
Age (years)						
≤ 65 (11)	54.7	37.2–72.3	Reference		Reference	
> 65 (14)	39.2	24.3–54.1	1.63 (0.48–5.59)	0.44	–	–
Stage at diagnosis						
≤ Stage III (19)	57.6	44.7–70.5	Reference		Reference	
Stage IV (6)	15.8	4.3–27.3	5.83 (1.63–20.92)	0.007	11.33 (2.07–37.37)	0.003
PWWP2B mutation						
Negative (17)	58.6	45.3–72.0	Reference		Reference	
Positive (8)	24.9	7.0–42.7	4.08 (1.19–14.00)	0.025	5.52 (1.45–20.97)	0.012

^aThe mean value is shown because of the small number of patients.

adenocarcinoma (Fig 1C; Cerami *et al*, 2012) and colorectal adenocarcinoma (Fig 1D; Giannakis *et al*, 2016) in cBioPortal (as of November 11, 2019) also showed mutation patterns comparable to ours. Next, we performed survival analysis to determine whether the *PWWP2B* mutation had a negative or positive effect on the prognosis of the disease. In this analysis, we found that the *PWWP2B* mutation was associated with poor patient prognosis with statistical significance. The mean overall survival (OS) duration of *PWWP2B*-mutation-positive patients was significantly shorter than that of the mutation-negative patients [mean, 24.9 (95% CI: 7.0–42.7) vs. 58.6 (95% CI: 45.3–72.0) months; HR = 4.08 (95% CI: 1.19–14.0); $P = 0.020$]. The survival rates at 12 and 24 months were 50 and 25% (mutation-positive) vs. 100 and 75% (mutation-negative), respectively ($P = 0.017$; 0.017; Fig 1E). The impact of the *PWWP2B* mutation on patient prognosis remained significant after adjusting for other variables by multivariate analysis (Table 1). Moreover, according to the Kaplan–Meier plot database, the low expression of *PWWP2B* was associated with worse overall survival in patients with stomach adenocarcinoma and lung cancer (Appendix Fig S2A and B; <http://kmpplot.com/analysis/>).

The *PWWP2B* is identified as a novel UHRF1 binding protein

To gain further insight into the molecular mechanisms of *PWWP2B* protein in the biological context, we performed tandem affinity purification using human embryonic a kidney (HEK) 293T cell line overexpressing SFB-*PWWP2B*. Mass spectrometry analysis identified

previously identified *PWWP2B*-binding proteins, including HDAC1/2 and human retinoblastoma-binding protein 4 (RBBP4; Zhang *et al*, 2018), which authenticated the validity of the proteomic analysis. Among the unknown interacting candidates, UHRF1 was selected for further studies since it was found to be the most promising *PWWP2B*-interacting protein with 37% of the coverage (Fig 2A). To confirm the interaction between *PWWP2B* and UHRF1, we performed immunoprecipitation assays using cells overexpressing SFB-*PWWP2B* and Myc-UHRF1 and found that *PWWP2B* was associated with UHRF1 (Fig 2B). The endogenous immunoprecipitation of *PWWP2B*-interacting proteins further proved that *PWWP2B* was associated with UHRF1 (Fig 2C). To determine the critical domains of *PWWP2B* responsible for UHRF1 binding, we generated a series of *PWWP2B* deletion mutants (Fig 2D) and co-transfected the individual GFP-*PWWP2B* deletion mutants with WT Myc-UHRF1 into HEK293T cells, followed by co-immunoprecipitation. The immunoprecipitation analysis showed that *PWWP2B* WT, -D1, -D4, and -D5 interacted with UHRF1, whereas the *PWWP2B*-D2 and -D3 mutants failed to do so, indicating that amino acid residues 130–317 of *PWWP2B* were important for its interaction with UHRF1 (Fig 2E). Next, we constructed a series of internal deletion mutants of UHRF1 as shown in Fig 2F (UHRF1-D1 to UHRF1-D5) to identify which regions of UHRF1 were important for its association with *PWWP2B* and found that the SRA (Set and Ring associated) domain of UHRF1 bound to *PWWP2B* (Fig 2G). These findings were further supported by the results showing that the GST-*PWWP2B*-N (Fig 2H and I, and Appendix Fig S3A), GST-*PWWP2B*-220, and -317 (Appendix Fig S4A)

Figure 1. Whole-exome sequencing analysis identifies genes recurrently mutated in stomach adenocarcinoma and somatic mutations in the *PWWP2B* gene.

- A Significantly recurrently mutated genes identified by MutSigCV analysis based on whole-exome sequencing data of 25 STAD patients' samples.
 B–D Distribution of *PWWP2B* mutations identified in 25 STAD patients (B). Distribution of *PWWP2B* mutations identified in the TCGA PanCancer Atlas stomach adenocarcinoma dataset (C; Cancer Genome Atlas Research Network, 2014). Distribution of *PWWP2B* mutations identified in a large-scale colorectal adenocarcinoma genomic study (D). PWWP (black box): PWWP domain.
 E Overall survival curve of 25 gastric cancer patients with and without *PWWP2B* mutations.

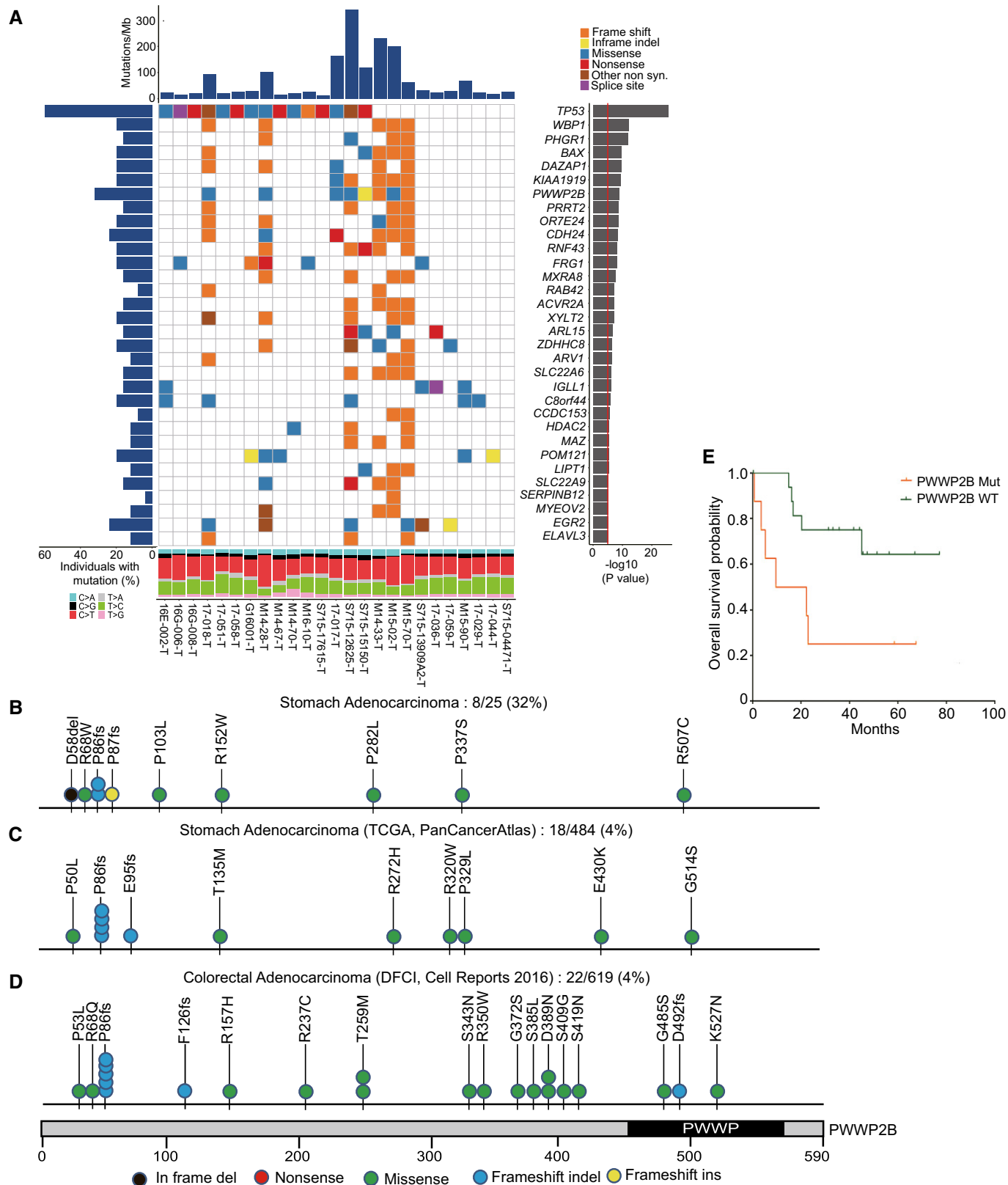


Figure 1.

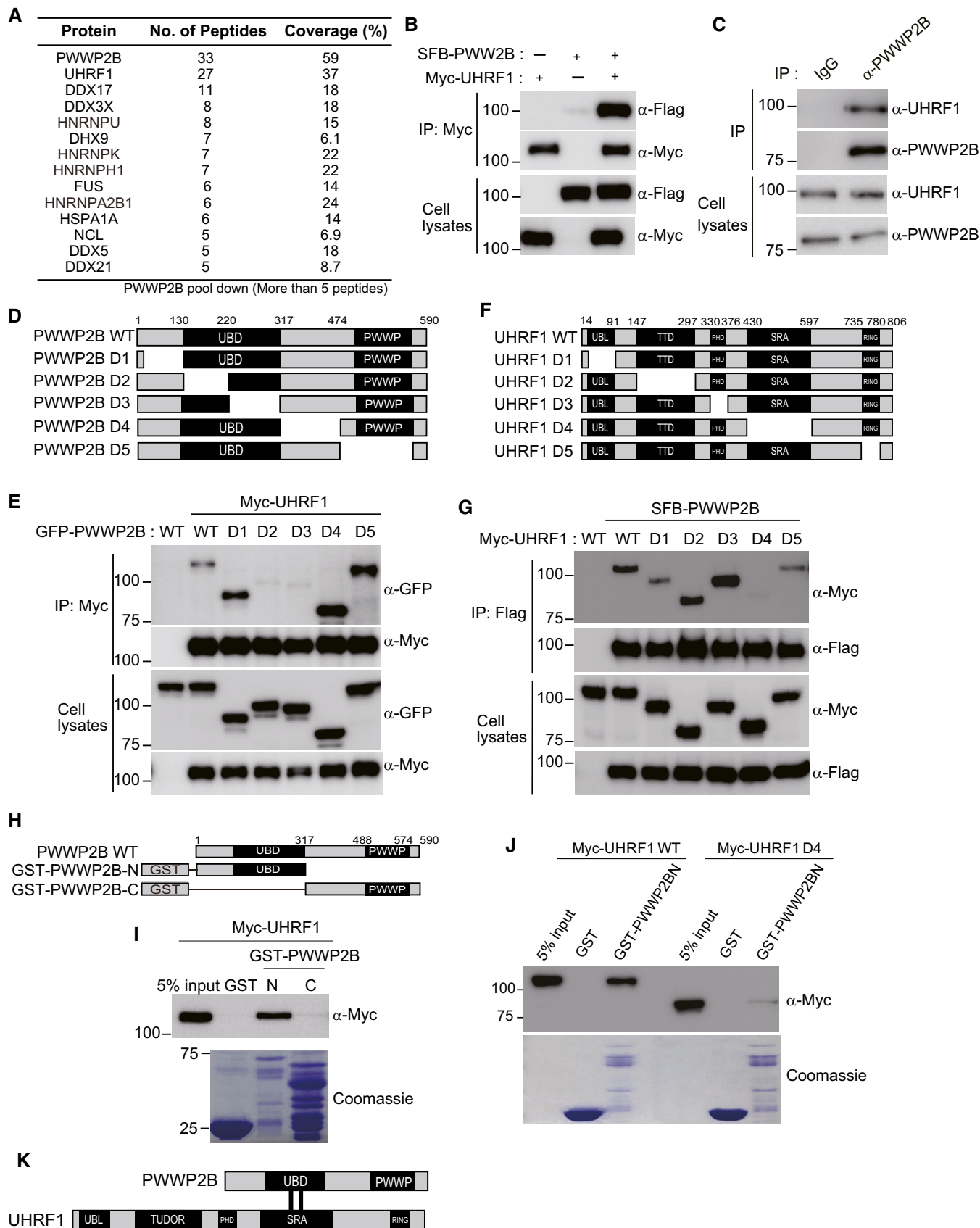


Figure 2.

Figure 2. PWWP2B is identified as a novel UHRF1-binding protein.

- A The list of proteins identified by mass spectrometric analyses of PWWP2B protein. The top 14 proteins co-purified with PWWP2B are shown.
- B The interaction between exogenous PWWP2B and UHRF1. The indicated plasmids were transfected into 293T cells. After 24 h, the transfected cell lysates were immunoprecipitated (IP) using an anti-Myc antibody and subjected to Western blotting analysis using the indicated antibodies. The bottom panel shows equal volumes of cell lysates immunoblotted with the indicated antibodies.
- C The interaction between endogenous PWWP2B and UHRF1. Immunoprecipitation reactions were performed using rabbit IgG or anti-PWWP2B antibodies and subjected to Western blotting analysis using the indicated antibodies. The bottom panel shows equal volumes of cell lysates immunoblotted with the indicated antibodies.
- D The upper panel shows a diagram of wild-type (WT) PWWP2B and serial deletion mutants (D1 to D5). The numbers indicate the amino acid residues. UBD, UHRF1 binding domain.
- E Myc-UHRF1 and either GFP-PWWP2B WT or its serial deletion mutants were co-transfected into 293T cells. The cell lysates were immunoprecipitated with the anti-Myc antibody and then immunoblotted with the indicated antibodies.
- F The upper panel shows a diagram of WT UHRF1 and its serial deletion mutants (D1 to D5). The numbers indicate the amino acids. UBL, ubiquitin-like domain; TTD, tandem Tudor domain; PHD, plant homeodomain; SRA, Set and RING associated; RING, really interesting new gene.
- G SFB-PWWP2B WT and either Myc-UHRF1 WT or its serial deletion mutants were immunoprecipitated with anti-FLAG and then immunoblotted with the indicated antibodies.
- H–J *In vitro* binding assay of PWWP2B and UHRF1. (H) Schematics of *PWWP2B* deletion mutants fused with glutathione S-transferase (GST). (I) Cell lysates of 293T cells transfected with Myc-UHRF1 expression vector were incubated with 2 μ g of purified GST, GST-PWWP2B-N, or GST-PWWP2B-C recombinant proteins for 1 h at 4°C. After pull-down with GST beads, the bound complexes were separated by sodium dodecyl sulfate–polyacrylamide gel electrophoresis (SDS–PAGE) and subjected to Western blot analysis using the indicated antibodies (upper panel). The Coomassie blue stain shows the purified GST fusion proteins. (J) Cell lysates of 293T expressing Myc-UHRF1 WT or Myc-UHRF1-D4 mutants were incubated with 2 μ g of purified GST or GST-PWWP2B-N for 1 h at 4°C. After pull-down with GST beads, the bound complex was analyzed by Western blots.
- K Schematic illustration of the binding domain architecture of PWWP2B and UHRF1.

fusion proteins were sufficient for UHRF1 interaction and that Myc-UHRF1-D4 was not sufficient for PWWP2B interaction (Fig 2J and Appendix Fig S3B). We also observed that the PWWP2B regions that contributed to binding with UHRF1 were highly conserved among species, implying that this region of PWWP2B likely has important biological functions (Appendix Fig S4B). Taken together, these data demonstrated that UHRF1 was associated with the PWWP2B protein through the UHRF1 binding domain (UBD; Fig 2K).

PWWP2B moves to sites of DNA damage through UHRF1 interaction

It has been reported that UHRF1 traveled to sites of DNA damage and played a role in DNA repair pathways (Tian *et al*, 2015; Zhang *et al*, 2016). As PWWP2B was identified as a new UHRF1 binding protein, we hypothesized that PWWP2B might translocate to the sites of DNA damage. To test this hypothesis, we took advantage of laser microirradiation that generates a limited amount of DNA damage in specified nuclear regions. GFP-tagged PWWP2B was constructed and expressed in HeLa cells. As shown in Fig 3A, GFP-PWWP2B accumulated at the DNA lesions generated by laser irradiation (Fig 3A) and also at the Fok1-induced DNA double-strand break (Appendix Fig S5A and B). In addition, accumulated GFP-PWWP2B on the laser stripes were colocalized with γ H2AX (Fig 3B), a marker for DNA damage, and also with UHRF1, in HeLa cells (Fig 3C). Having the PWWP2B antibody, we further confirmed that the endogenous PWWP2B accumulates at the sites of laser-induced DNA lesions (Fig 3D). To study the kinetics of the recruitment of PWWP2B and UHRF1 to DNA lesions, we used real-time imaging techniques to monitor protein accumulation at the laser stripes upon microirradiation. We found that both GFP-UHRF1 and mCherry-PWWP2B rapidly translocated to the DNA-damage sites within 1 min after laser microirradiation (Fig 3E). Notably, we observed that the accumulation of GFP-UHRF1 and mCherry-PWWP2B at the DNA damage sites peaked at 3 min and then

remained steady up to 20 min with similar kinetics (Fig 3E), suggesting that both UHRF1 and PWWP2B play important roles in the early stage of DDR and continued to exert their effects in the remaining DDR processes. Next, we determined the specific regions of PWWP2B responsible for its translocation to the DNA damage sites. To this end, we generated a series of GFP-tagged PWWP2B WT and deletion mutants (D1, D2, D3, D4, and D5) and then transiently expressed the individual clones in HeLa cells (Fig 3F). HeLa cells expressing the individual clones were irradiated, and the cells with positive GFP on laser stripes were counted. We found that about 80% of the cells expressing the PWWP2B WT or D1 mutant, and about 55% of the cells expressing the PWWP2B D5 mutant. However, GFP-PWWP2B D2 and D3 were barely localized to the laser stripes indicating that the PWWP2B domains responsible for UHRF1 interaction were critical for PWWP2B localization to the sites of DNA damage (Fig 3F). We noticed that amino acid residues 317–474 of PWWP2B, which were not responsible for UHRF1 interaction, were also important for the recruitment of PWWP2B to the sites of DNA damage as the GFP-PWWP2B-D4 failed to localize to the laser stripes. To exclude the possibility that altered protein conformational changes caused the inability of the PWWP2B D2 and D3 mutants to localize to the laser stripe, we generated GFP-PWWP2B-A2A3 mutants (Fig 3G), and then tested the recruitment of the 130–317 amino acids of PWWP2B upon microirradiation (Fig 3H). The microirradiation assay data showed that amino acids 130–317 of PWWP2B (A2A3 mutant) were solely sufficient for its localization to the laser stripe (Fig 3H). The results showing that amino acids 130–317 (A2A3 deletion mutant) of PWWP2B were important both for binding with UHRF1 and the localization to the DNA damage sites suggest that the localization of PWWP2B to the sites of DNA damage was dependent upon the interaction with UHRF1. However, the GFP-PWWP2B-A4 clone did not move to the laser stripes (Fig 3H), implying that both PWWP2B-UHRF1 interaction and amino acid residues 317–474 were required for the proper recruitment of PWWP2B to the sites of DNA damage (Fig 3G and H). To test whether UHRF1 controlled the localization of PWWP2B

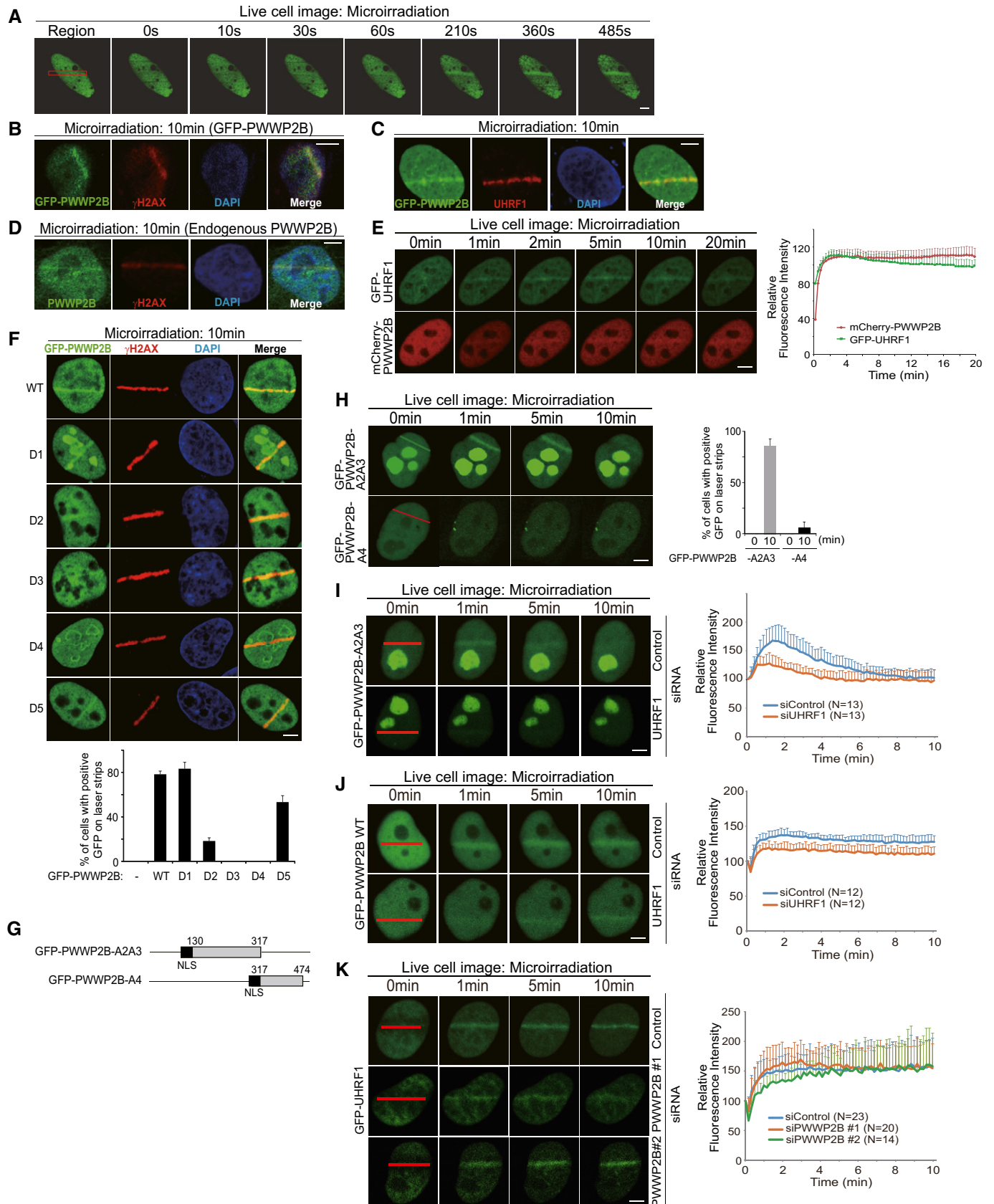


Figure 3.

Figure 3. PWWP2B is recruited to DNA damage sites.

- A HeLa cells expressing GFP-PWWP2B were subjected to laser microirradiation. The laser stripes were examined at the indicated time points. Scale bar, 5 μm .
- B, C HeLa cells expressing GFP-PWWP2B were subjected to laser microirradiation. After 10 min, the cells were fixed and stained with anti-GFP and anti- γH2AX (B) or anti-UHRF1 antibodies (C). 4',6-diamidino-2-phenylindole (DAPI) was used to stain the nucleus. Scale bar, 5 μm .
- D HeLa cells were treated with laser microirradiation. After 10 min, the cells were fixed and stained with anti-PWWP2B and anti- γH2AX antibodies. Scale bar, 5 μm .
- E Comparison of the translocation kinetics for GFP-UHRF1 and mCherry-PWWP2B to the sites of DNA damage. HeLa cells expressing both GFP-UHRF1 and mCherry-PWWP2B were subjected to laser microirradiation. (left panel). Scale bar, 5 μm . The laser stripes were examined at the indicated time points. The intensity of each laser stripes in each time point was measured by averaging values from 10 cells and graphed in the right panel. The error bars indicate the standard deviation (SD).
- F HeLa cells were transfected with GFP-PWWP2B WT or deletion mutant expression plasmids, and 24 h later, the cells were treated with laser microirradiation (top panel). Scale bar, 5 μm . The cells with positive GFP expression on the laser stripes are presented in the bar graph (bottom panel). The results represent the average of three independent experiments. The error bars indicate the standard deviation.
- G Diagram of the deletion mutants (A2A3 and A4). The numbers indicate the amino acids in PWWP2B.
- H GFP-PWWP2B-A2A3 deletion mutant translocates to the DNA damage sites. HeLa cells were transfected with GFP-tagged deletion mutant expression plasmids, and 24 h later, the cells were treated with laser microirradiation (left panel). Scale bar, 5 μm . The cells with positive GFP expression on the laser stripes after 10 min were counted and presented in the bar graph (right panel). The results represent the average of three independent experiments. The error bars indicate the standard deviation for the cells transfected with each expression plasmid.
- I, J HeLa cells depleted with either control or UHRF1 siRNAs were transfected with the GFP-PWWP2B-A2A3 (I) and GFP-PWWP2B WT (J) expression plasmid. After 24 h, the cells were subjected to laser microirradiation. Scale bar, 5 μm . The laser stripes were examined at the indicated time points. The intensity of each laser stripes in each time point was measured by averaging values from indicated number of cells and graphed in the right panel. The error bars indicate the standard deviation.
- K HeLa cells depleted with either control or PWWP2B siRNA were transfected with GFP-UHRF1 expression plasmids. After 24 h, the cells were subjected to laser microirradiation. Scale bar, 5 μm . The laser stripes were examined at the indicated time points. The intensity of each laser stripes in each time point was measured by averaging values from indicated number of cells and graphed in the right panel. The error bars indicate the standard deviation.

to the DNA damage sites, we performed a microirradiation assay upon UHRF1 depletion. Surprisingly, the accumulation of the PWWP2B A2A3 mutant and wild-type PWWP2B at the laser stripes was dramatically impaired in the UHRF1-depleted cells (Fig 3I and J), whereas the accumulation of UHRF1 at the laser stripes was not impaired in PWWP2B-depleted cells (Fig 3K), indicating that UHRF1 likely acted upstream of PWWP2B in DDR. Collectively, these findings demonstrate that PWWP2B translocated to the sites of DNA damage through its interaction with UHRF1 and likely exerted its effects downstream of UHRF1.

PWWP2B plays important roles in the DNA double-strand break repair pathway

Next, we examined the possible functions of PWWP2B in the DNA repair pathways. First, we found that the damage-induced γH2AX foci slowly disappeared in PWWP2B-depleted HeLa cells upon ionizing radiation (IR) compared to the cells treated with control siRNA (Fig 4A and Appendix Fig S6). This result raised the possibility that PWWP2B participated in repairing DSBs. There are two major pathways of DSB repair, HR and NHEJ. We tested which DSB repair pathway PWWP2B participated in. From the results of the GFP-based reporter assays, we found that the efficiency of HR repair was significantly reduced in cells treated with siPWWP2B (Fig 4B and Appendix Fig S7A–C). However, in the same setting, the NHEJ capacity was mildly affected by PWWP2B depletion (Fig 4C and Appendix Fig S7D), demonstrating that PWWP2B functioned primarily in the HR pathway in these cells. It was reported that UHRF1 is recruited to the site of DNA damage in S-phase (Zhang *et al*, 2016) when HR primarily takes place. Consistently, we confirmed that PWWP2B was also recruited to DNA damage sites in S phase (Appendix Fig S8). These findings were further supported by the fact that the IR-induced foci formation of RAD51, an important HR protein, was severely impaired in the PWWP2B-depleted cells at S cell cycle phase (Fig 4D, and Appendix Figs S9 and S10A). To remove the off-targeting effects of siRNA-mediated knockdown (KD) of PWWP2B, rescue experiments were conducted using the

siRNA-resistant PWWP2B WT expression vector (Appendix Fig S11A and B). The reconstitution of PWWP2B WT in PWWP2B-KD cells successfully restored IR-induced RAD51 foci formation (Fig 4E). Along with these results, we also observed that IR-induced BRCA1 foci formation decreased in PWWP2B-depleted cells at the S phase (Fig 4F and Appendix Fig S10B), whereas IR-induced 53BP1 (Fig 4G and Appendix Fig S10C), γH2AX , ubiquitin, MDC1, or RAP80 foci formation were not altered by these conditions (Appendix Fig S12). These results suggest that PWWP2B protein played roles in DSB repair through promoting the recruitment of HR factors to the DNA damage sites. Next, we tested the effects of PWWP2B depletion on the clonogenic survival of HeLa cells in response to IR. Remarkably, PWWP2B depletion rendered the cells more sensitive to IR compared to the control KD cells (Fig 4H). These results suggest that PWWP2B was required to promote HR for cell survival in response to IR-induced DNA damage.

End resection is severely impaired in PWWP2B-depleted cells

As shown in Fig 4D, PWWP2B was critical for damage-induced RAD51 foci formation, which suggests that PWWP2B might function in the end resection step during HR. Furthermore, we confirmed that these observations were bona fide phenotypes of PWWP2B depletion by validating the expression level of RAD51, RPA2, and BRCA1 proteins in PWWP2B-KD cells (Fig 5A and B). To further understand the roles of PWWP2B in end resection, we examined the accumulation of replication protein A (RPA) in response to DNA damage. Replication protein A is phosphorylated and bound to ssDNA, which is generated after end resection at the sites of DNA DSBs. Interestingly, the depletion of PWWP2B leads to severe decreases in RPA phosphorylation in response to DNA damage induced by IR (Fig 5B and Appendix Fig S13). Similarly, we found that the damage-induced foci formation of RPA2 and phosphorylation of RPA2 S4/S8 were significantly impaired in cells treated with siPWWP2B (Fig 5C and D). To confirm the defects in end resection more accurately *in vivo*, we employed a PCR-based method allowing us to measure a fraction of the resected DNA at the defined

double-stranded DNA (Fig 5E). As shown in Fig 5F, the depletion of PWWP2B resulted in a significant decrease in DNA end resection at the same level of MRE11 depletion. Taken together, these findings demonstrated that PWWP2B played a critical role in end resection during HR.

PWWP2B is associated with MRE11

Next, we wanted to understand the molecular basis of how PWWP2B regulates DNA end resection. As shown in Appendix Fig S12, we

noticed that damage induced foci formation of γ H2AX, ubiquitin, MDC1 and RAP80, regulating the DNA damage response, was normal in the absence of PWWP2B. Therefore, we tested if nucleases or nuclease-associated factors for end resection were targeted to the sites of DNA damage. Interestingly, we found that the irradiation-induced MRE11 foci formation was severely impaired in PWWP2B-depleted cells (Fig 6A). As expected, there were severe defects in irradiation-induced MRE11 foci formation in HeLa cells depleted with UHRF1 which functions upstream of PWWP2B. Consistently, the laser microirradiation assay showed that the

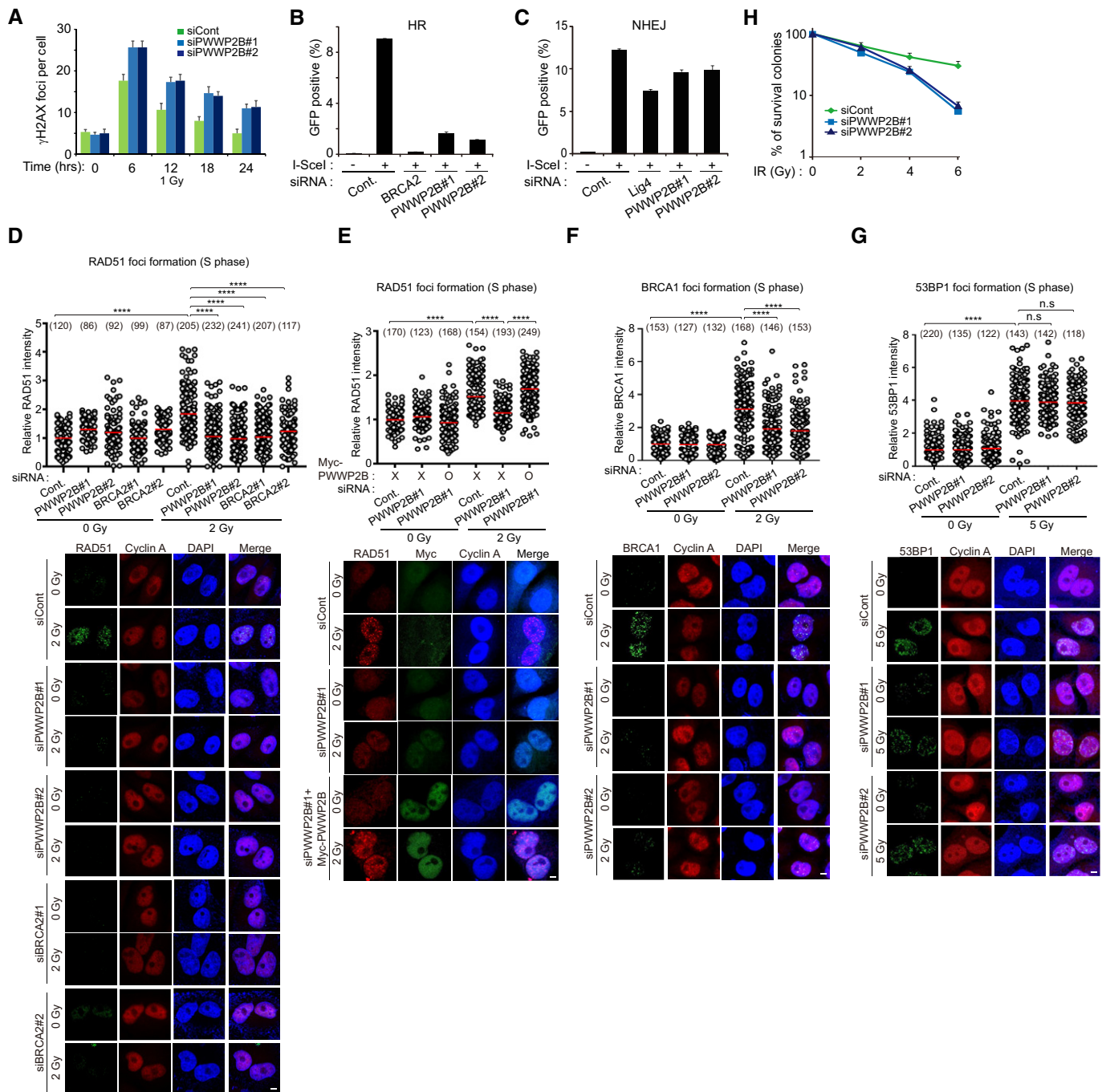


Figure 4.

Figure 4. PWWP2B is implicated in DDR and HR-mediated DSB repair.

- A** The numbers of γ H2AX foci at the indicated time points after exposure to 1 Gy of ionizing radiation (IR) in HeLa cells transfected with either control or PWWP2B siRNA1 or 2. The results represent the average of three independent experiments. More than 50 cells were examined for each condition. The error bars indicate the standard deviation for cells transfected with each siRNA.
- B, C** Measurement of homologous recombination and non-homologous end-joining capacity in DR-GFP and EJ5-GFP reporter U2OS cells. (B) U2OS cells harboring the DR-GFP reporter were treated with the indicated siRNAs, followed by transfection with the I-SCE1 expression vector. Two days later, GFP expression was accessed by flow cytometry. BRCA2 depletion was used as a negative control. (C) The NHEJ assay was performed with U2OS cells harboring the NHEJ reporter (EJ5-GFP). The reporter cells were transfected with the indicated siRNAs, followed by transfection with the I-SCE1 expression vector. Two days later, the GFP-expressing cells were accessed by flow cytometry. LIG4 depletion was used as a negative control. The GFP expression levels are shown as the average of three independent experiments, and the error bars indicate the standard deviation.
- D–G** Quantification of radiation-induced RAD51, BRCA1, and 53BP1 foci formation in HeLa cells treated with the indicated siRNAs. All data were obtained from over 85 cells (open circles), and the mean values are shown as red bars (upper panel). Immunofluorescence analysis of irradiation-induced RAD51, BRCA1, and 53BP1 foci formation. HeLa cells transfected with either control or PWWP2B siRNAs were synchronized in S phase by a double thymidine block and exposed to 0 or 2 Gy of IR. The cells were incubated for 2 h, fixed, and subjected to staining with RAD51 (D and E), BRCA1 (F), or 53BP1 (G) antibodies. The cells in S phase were identified by Cyclin A staining. (E) The siPWWP2B-resistant PWWP2B WT expression vector was transfected into HeLa cells after siRNA-mediated PWWP2B depletion. IR-induced RAD51 foci formation was examined by immunofluorescence. Scale bar, 5 μ m. The *P*-values are determined by one-way ANOVA. *****P* < 0.0001, n.s., not significant.
- H** Cell survival of the PWWP2B-depleted HeLa cells in response to IR. HeLa cells were transfected with either control or PWWP2B siRNAs. After 48 h of transfection, 500 cells were plated and irradiated with the indicated doses of IR. The number of surviving colonies was counted 14 days after IR exposure. These experiments were performed in triplicate, and the results represent the average of three independent experiments. The error bars indicate the standard deviation.

recruitment of GFP-MRE11 on laser stripes was significantly impaired in PWWP2B depleted HeLa cells (Fig 6B). MRE11 defects were further confirmed by the impaired ATM activation in cells treated with siRNA against PWWP2B (Appendix Fig S14). These findings prompted us to test if PWWP2B was associated with MRE11. To this end, immunoprecipitation was performed using lysates prepared from HEK293T cells expressing HA-PWWP2B and Myc-MRE11. As shown in Fig 6C, we found that Myc-MRE11 was co-immunoprecipitated with HA-PWWP2B. The interaction was confirmed between endogenous PWWP2B and MRE11 (Fig 6D). To determine the PWWP2B domains responsible for MRE11 interaction, we transfected GFP-PWWP2B and its deletion mutants with HA-MRE11 and found that the amino acid residues 130–220 and 474–580 of PWWP2B were important for PWWP2B and MRE11 interaction (Fig 6E). Taken together, these findings demonstrated that PWWP2B regulated MRE11 recruitment to the sites of DNA damage and thus, played an important role in end resection during HR.

UHRF1 and PWWP2B are epistatic in DDR and HR-mediated DSB repair

Depletion of UHRF1 impairs HR, end-resection and MRE11 recruitment to the sites of DNA damage. To test if the defects are mediated by UHRF1-PWWP2B interaction, we introduced siRNA-resistant wild-type UHRF1 in the HeLa cells depleted with UHRF1 and found that those defects were rescued. However, expression of siRNA-resistant UHRF1-D4, which does not interact with PWWP2B, failed to do so, demonstrating that UHRF1 plays roles in HR through PWWP2B interaction (Appendix Fig S15A–C). These results suggested that PWWP2B was likely epistatic to UHRF1 in DDR and HRR. To prove this possibility, we tested the effects of the genetic interaction between PWWP2B and UHRF1 on DDR and HR by depleting either PWWP2B, UHRF1, or both. We found that either the individual or dual depletion of PWWP2B and UHRF1 resulted in a similar level of defects in IR-induced γ H2AX, RAD51, and BRCA1 foci formation, indicating that PWWP2B and UHRF1 were epistatic for DDR and HRR (Fig 7A–C). In addition, PWWP2B was epistatic to UHRF1 in IR sensitivity (Fig 7D and Appendix Fig S16A) and the homology mediated the DSB repair pathway (Fig 7E and Appendix

Fig S16B). The depletion of individual or combined PWWP2B and UHRF1 did not affect the protein expression level of BRCA1, 53BP1, and RAD51, indicating that neither protein regulated the gene expression profiles of factors implicated in DDR and HRR (Appendix Fig S16C). To identify the specific regions of PWWP2B important for the function of PWWP2B in DDR, we generated siRNA-resistant PWWP2B WT and deletion mutants. Restoration experiments using the siRNA-resistant PWWP2B WT and its serial deletion mutants showed that the defect in IR-induced RAD51 foci formation in PWWP2B-KD cells was restored by the expression of siRNA-resistant PWWP2B WT, but not by the expression of PWWP2B-D2, -D3, or -D4 mutants (Appendix Fig S17A). Consistently, the hypersensitivity of PWWP2B-KD cells to IR was also restored by the re-expression of siRNA-resistant PWWP2B WT, whereas the expression of PWWP2B-D2, -D3, and -D4 failed to be restored (Appendix Fig S17B). Taken together, these data strongly suggest that PWWP2B was located to the sites of DNA damage to promote HR and that PWWP2B was likely an epistatic factor to UHRF1 in DDR and HR-mediated DSB repair in these cells.

Discussion

HR-mediated DSB repair is critical for cell survival and maintaining genomic integrity in response to a variety of DNA damage. In this study, we investigated the roles of PWWP2B in the DNA damage response and DSB repair. We demonstrated that PWWP2B was dispatched to the sites of DNA DSBs through its association with UHRF1 and that PWWP2B was a novel factor implicated in HR-mediated DSB repair. We also showed that PWWP2B was associated with MRE11, which promoted end resection at the sites of DNA DSBs. Of note, the mutation status of the *PWWP2B* gene and the level of PWWP2B mRNA expression exhibited a significant association with STAD incidence and the overall survival of cancer patients. The low expression of PWWP2B mRNA in stomach adenocarcinoma and lung cancer was correlated with worse overall patient survival according to the Kaplan–Meier plot (Appendix Fig S2A and B). In addition, our clinical data showed that the gastric adenocarcinoma patients bearing mutations in *PWWP2B* had shorter

overall survival compared to patients with wild-type *PWWP2B* (Fig 1E). These data imply that *PWWP2B* possibly plays a role in cancer progression and therefore *PWWP2B* could be added to the list of diagnostic marker of STAD.

Among all types of DNA damage, DSBs are considered the most harmful threat to genomic integrity and cell viability. If DSBs are not properly repaired, they will cause genomic instability and, consequently, various diseases, including cancer. Cells activate the DDR,

a complex signaling network that modulates cell cycle progression, transcription, DNA repair, and cell survival in response to DSBs (Harper & Elledge, 2007). A number of DDR factors translocate to the DNA damage sites to regulate DSB repair. Among them, UHRF1 localized to DNA damage sites was shown to regulate the DSB repair pathway choice by regulating RIF1 ubiquitination, thus channeling repair to the HR pathway (Zhang et al, 2016). In this study, *PWWP2B* bound to UHRF1 (Fig 2) and, upon microirradiation, was

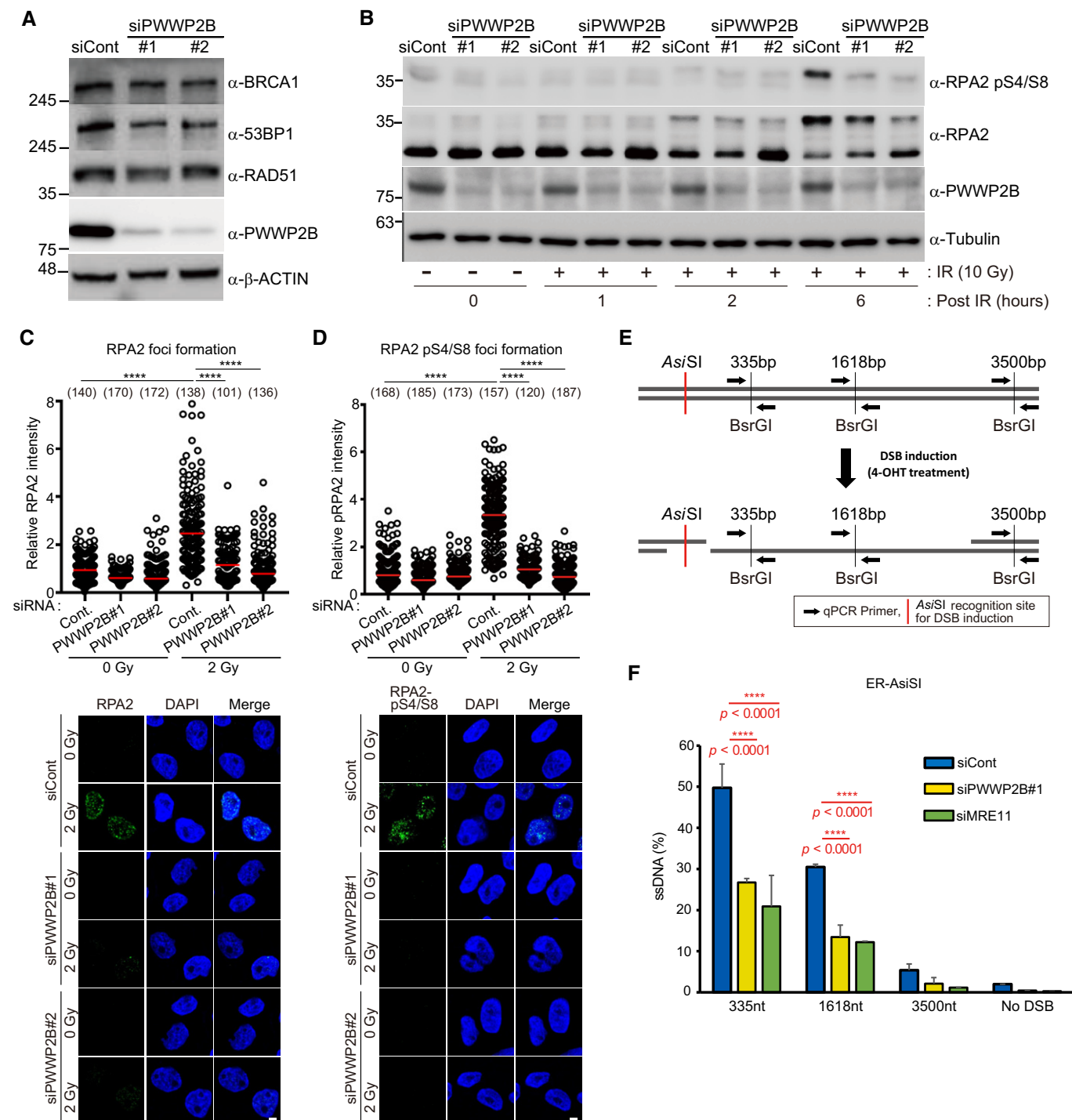


Figure 5.

Figure 5. PWWP2B participates in DNA end resection during HR.

- A Immunoblot analysis of RAD51, BRCA1, or 53BP1 protein levels in PWWP2B-depleted HeLa cells.
- B RPA phosphorylation at the indicated time points in response to IR exposure. HeLa cells treated with the indicated siRNAs were irradiated and the lysates prepared at the indicated time points were subjected to immunoblot analysis for the presence of S4/S8 phosphorylation and total RPA.
- C, D Quantification of radiation-induced RPA2 or S4/S8 phosphorylated RPA foci formation in PWWP2B-depleted HeLa cells. All data were obtained from over 100 cells (open circles), and the mean values are shown as red bars (upper panel). The *P*-values are determined by one-way ANOVA. *****P* < 0.0001. Immunofluorescence analysis of irradiation-induced RPA2 or S4/S8 phosphorylated RPA2 foci formation. HeLa cells treated with either control or PWWP2B siRNAs were exposed to 0 or 2 Gy of IR. The cells were incubated for 2 h, fixed, and subjected to staining with RPA2 (C), or S4/S8 phosphorylation-specific RPA2 (D) antibodies (bottom panel). Scale bar, 5 μ m.
- E Schematic illustration of the quantitation of DNA resection in human cells by the ER-AsiSI assay. The AsiSI site located on chromosome 1 is indicated as a red bar. Three pairs of qPCR primers were designed crossing the BsrGI restriction sites and the distances from the AsiSI sites are written as numbers.
- F ER-AsiSI U2OS cells were transfected with the indicated siRNAs. Two days after transfection, the cells were treated with 300 nM 4-OHT for 4 h, then the genomic DNA from those cells was extracted and digested with BsrGI overnight. DNA end resection near the AsiSI site was measured by qPCR as described in the Materials and Methods. The results are the average of three experiments and the error bars indicate standard deviations. The *P*-values are determined by one-way ANOVA. *****P* < 0.0001.

mobilized to DNA damage sites and co-localized with UHRF1 (Fig 3). Its UHRF1 interaction-defective mutations failed to migrate to the DNA damage sites (Fig 3). The depletion of PWWP2B also exhibited reduced RAD51 foci formation and reduced cell survival after IR treatment (Fig 4). These results demonstrate the functions of PWWP2B in DDR and HR-mediated DSB repair in collaboration with UHRF1. For HR initiation, DSBs are first recognized by the MRN complex, and then DNA end resection takes place to generate 3' ssDNA overhangs. This step is critical for the initiation of HR. BRCA1 and UHRF1 cooperate to promote HR (Zhang *et al*, 2016) and BRCA1 was shown to promote CtIP-mediated DNA end resection (Cruz-Garcia *et al*, 2014). Depletion of PWWP2B led to reductions in IR-induced BRCA1 foci formation, suggesting that PWWP2B functions in recruiting BRCA1 to the sites of DSBs (Fig 4F). Additionally, PWWP2B depletion showed reductions in RPA2 foci formation and pRPA2 (S4/S8) phosphorylation in response to IR (Fig 5B–D), hinting that PWWP2B participated in DNA end resection. Additionally, we found that PWWP2B promotes end resection through direct interaction with MRE11. Damage-induced MRE11 foci formation was severely impaired in cells depleted with PWWP2B. It was reported that depletion of MRE11 leads to attenuated ATM activation (Lee & Paull, 2004; Li *et al*, 2017; Wang *et al*, 2019), and increased unrepaired DNA damage and the DNA damage marker, γ H2AX at later time point (Kondratova *et al*, 2015). Consistently, we found that depletion of PWWP2B results in impairment of DNA damage-induced ATM phosphorylation at S1981 (Appendix Fig S14). However, interestingly, we noticed that damage-induced γ H2AX foci were increased at the later time points in the absence of PWWP2B (Fig 4A). Similarly, we found that irradiation-induced foci formation of γ H2AX, MDC1, ubiquitin, and RAP80 foci formation is normal (Appendix Fig S12). These results might be due to the DNA-PKcs functions, which is also able to phosphorylate H2AX in response to DNA damage (Goldberg *et al*, 2003; Stiff *et al*, 2004). This is why we observed not severely impaired DNA damage response in the absence of PWWP2B.

PWWP2B was identified as an interacting protein of H3K36me3, a histone modification on active chromatin, and enriched at the promoters and enhancers of highly active genes in mouse ES cells (Zhang *et al*, 2018). It was proposed that PWWP2B plays a role in transcriptional regulation via finely modulating the dynamics of histone acetylation at genes actively transcribed. Besides its roles in the transcriptional regulation, H3K36 methylation has been shown

to be a critical chromatin component of DDR and linked to DNA repair in the regions of active transcription (Aymard *et al*, 2014; Pfister *et al*, 2014). For example, H3K36me3 provided interacting sites on the PWWP domain of LEDGF (p97), which facilitated HRR via its association with CtIP (Daugaard *et al*, 2012). PWWP2B was associated with H3K36me3 at actively transcribed genes (Zhang *et al*, 2018) and important for HR-mediated DNA repair (Figs 4 and 5), thus raising the possibility that PWWP2B plays roles in DDR and DSB repair in the regions of active genes through regulating the status of chromatin modification. Consistent with this possibility, we noticed that PWWP2B-D5 deletion mutant lacking the PWWP domain showed reduced localization on the laser stripes by about 50% (Fig 3F), implying that the PWWP domain of PWWP2B might play a role in recognizing alternative DNA structure often found at sites of DNA damage. This scenario needs to be investigated in future studies. PWWP2B consists of two functional domains, the UHRF1-binding domain (UBD) and the PWWP domain (Fig 2K). We found that the PWWP2B UBD domain responsible for the interaction with UHRF1 was critical for the functions of PWWP2B in DDR and HR-mediated DSB repair in response to IR (Fig 3F and Appendix Fig S17A and B). Interestingly, the UBD domain was solely sufficient for translocation to the sites of DNA lesions upon microirradiation (Fig 3H), emphasizing the functional importance of the interaction between PWWP2B and UHRF1 on DDR and HR-mediated DSB repair. Besides interaction regions (UBD, 130–317 aa), we found that the adjacent region (317–374) also played an important role in RAD51 foci formation and cell survival in response to IR. However, contrary to the A2A3 region, the A4 region fails to move to the laser stripes implying that the A4 region itself is not sufficient for the PWWP2B localization to the sites of DNA damage. It is possible that the A4 region, together with the PWWP domain, might be required for recognizing the DNA lesion substrates. This possibility needs to be investigated in future studies.

Some DDR factors, including UHRF1, have been reported to perform important roles in response to various types of DNA damage. Besides the functions of UHRF1 in DSB repair, it has been shown to play roles in the repair of DNA interstrand crosslinks (ICLs) through sensing ICLs and locating FANCD2 to ICL lesions to initiate Fanconi anemia pathway, a major pathway of ICL repair (Liang *et al*, 2015; Tian *et al*, 2015). We showed that PWWP2B interacted with UHRF1 and that the interaction was critical for its recruitment to DNA damage sites for DNA repair and cell survival in response to IR.

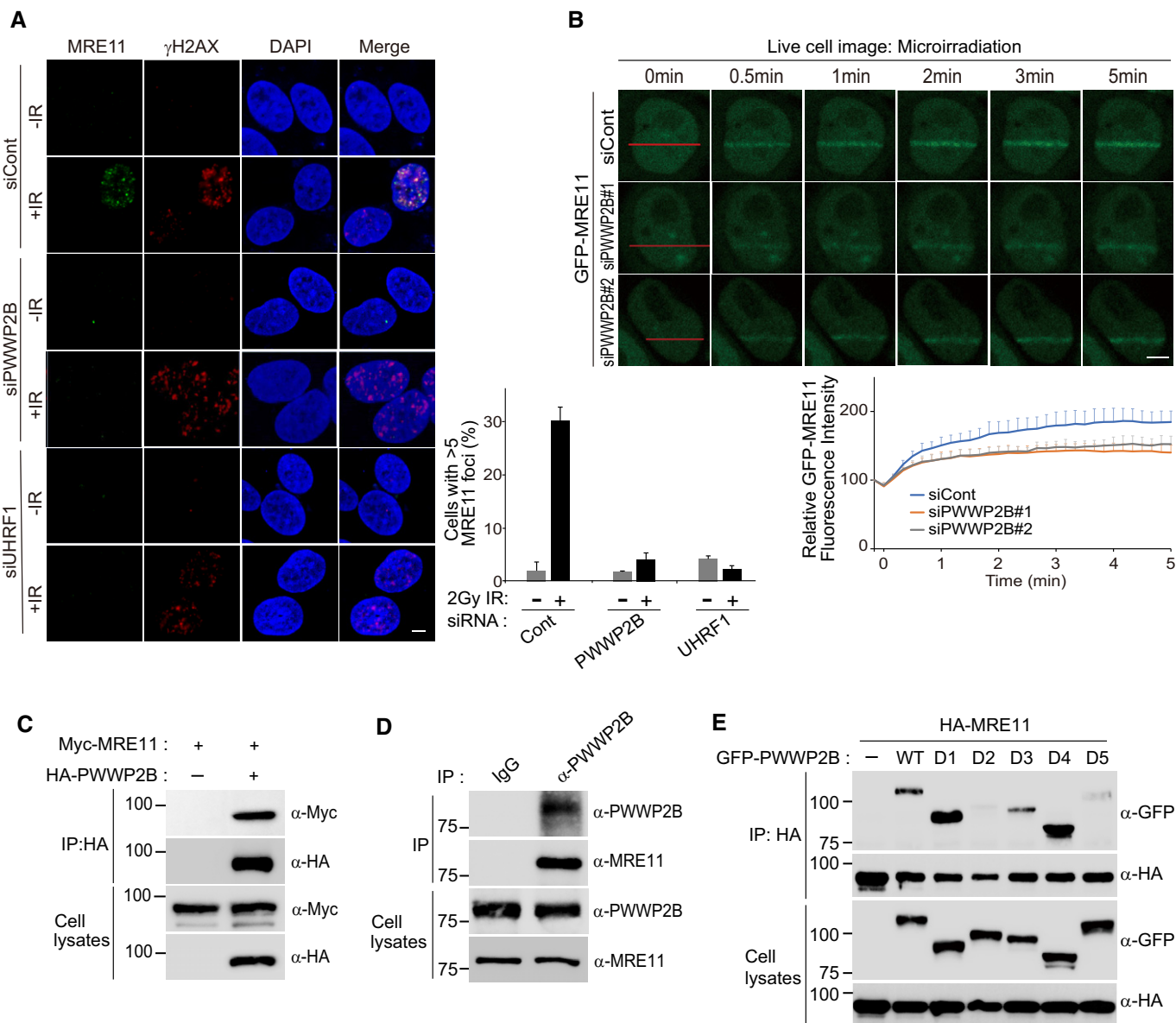


Figure 6. PWWP2B is associated with MRE11.

A Immunofluorescence analysis for irradiation-induced MRE11 foci formation (left panel). HeLa cells transfected with either control siRNA, siPWWP2B, or siUHRF1 were irradiated, fixed, and subjected to staining with MRE11 and γ H2AX antibodies. More than 100 nuclei per condition were counted. Scale bar, 5 μ m. The percentage of MRE11-positive cells is presented as a bar graph (right panel). The results represent the average of three independent experiments. The error bars indicate standard deviation.

B HeLa cells expressing GFP-MRE11 were treated with control siRNA or siRNAs against PWWP2B. After 48 h, the cells were subjected to laser microirradiation. Stripes on the laser were examined at the indicated time points (upper panel). Scale bar, 5 μ m. The intensity of the laser stripes at the time points was determined. The average intensity values from 10 cells were graphed in the bottom panel. The error bars indicate standard deviation.

C The interaction between PWWP2B and MRE11. HA-PWWP2B and Myc-MRE11-expressing vectors were transfected into 293T cells. After 24 h, the cell lysates were immunoprecipitated with anti-HA antibody, followed by immunoblot analysis with the indicated antibodies.

D The interaction between endogenous PWWP2B and MRE11. Immunoprecipitation reactions were performed using rabbit IgG or anti-MRE11 antibodies, followed by immunoblot analysis with the indicated antibodies. The bottom panel shows equal volumes of cell lysates immunoblotted with the indicated antibodies.

E HA-MRE11 and either GFP-PWWP2B WT or its serial deletion mutants were co-transfected into 293T cells. The cell lysates were immunoprecipitated with anti-HA antibody and then immunoblotted with the indicated antibodies.

Therefore, whether PWWP2B has roles in other DNA repair pathways should be determined.

In this study, we demonstrated that PWWP2B was one of the frequently mutated genes in Korean gastric adenocarcinoma patient

tissues through WES and analysis by bioinformatics tools. We also showed that PWWP2B participated in DDR and HR-mediated DSB repair by interacting with UHRF1, a known important factor for DDR and DSB repair pathway choice (Zhang *et al*, 2016). In

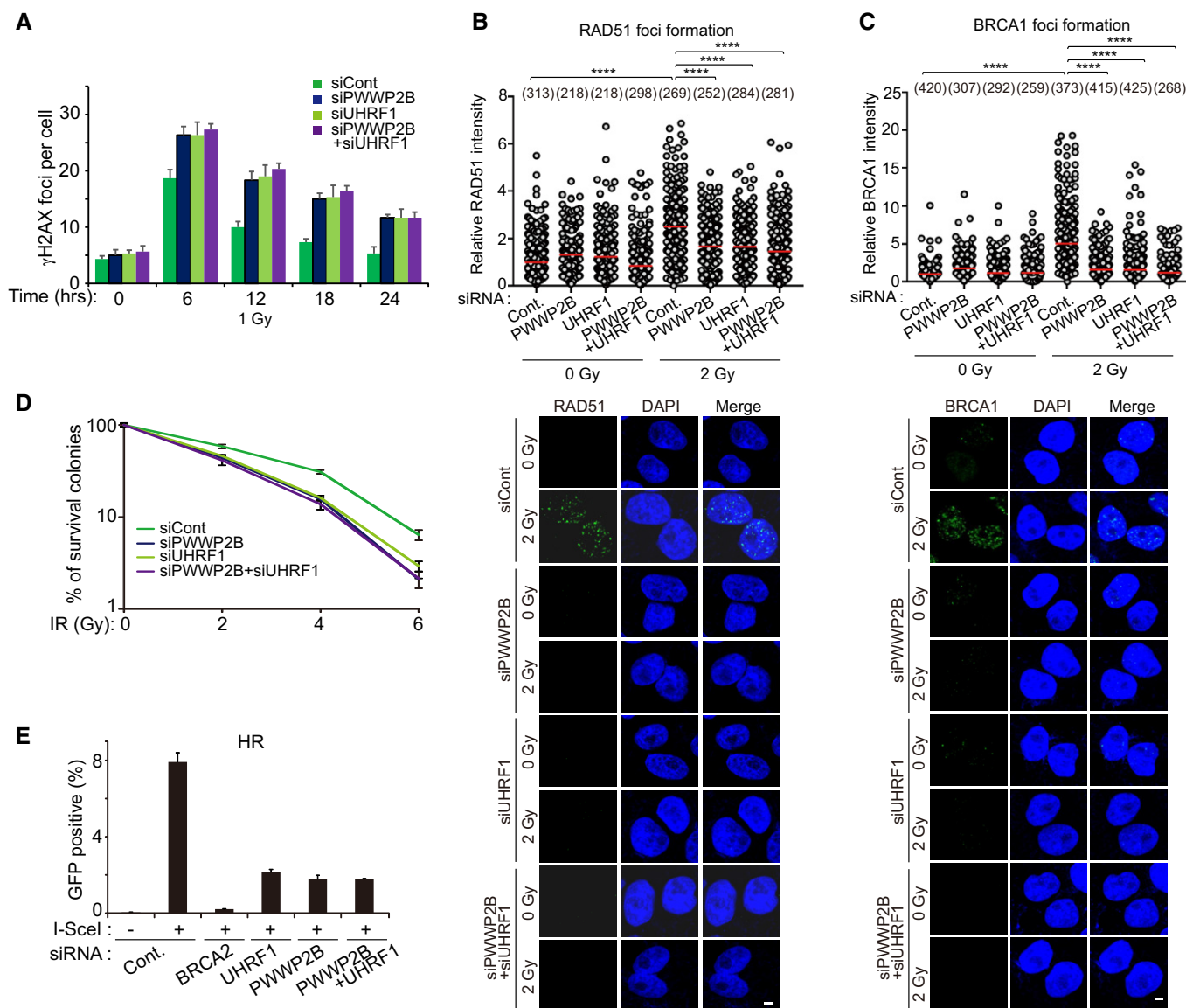


Figure 7. PWWP2B and UHRF1 are epistatic in DDR and HR-mediated DSB repair.

A Comparison of IR-induced γ H2AX foci formation in HeLa cells treated with the indicated siRNAs. γ H2AX foci were counted at the indicated time points after exposure to 1 Gy of ionizing radiation (IR) in HeLa cells transfected with the indicated siRNAs. The results represent the average of three independent experiments. More than 50 cells were examined for each condition. The error bars indicate the standard deviation for cells transfected with the indicated siRNAs.

B, C Comparison of IR-induced foci formation for either RAD51 or BRCA1 in HeLa cells transfected with the indicated siRNAs. Quantification of radiation-induced RAD51 or BRCA1 foci formation in PWWP2B alone, UHRF1 alone, or PWWP2B and UHRF1-depleted HeLa cells. All data were obtained from over 100 cells (open circles), and the mean values are shown as red bars (upper panel). The *P*-values are determined by one-way ANOVA. *****P* < 0.0001. Immunofluorescence analysis of irradiation-induced RAD51 or BRCA1 foci formation. HeLa cells treated with the indicated siRNAs were exposed to 0 or 2 Gy of IR. The cells were incubated for 2 h, fixed, and subjected to staining with RAD51 (B), or BRCA1 (C) antibodies (bottom panel). Scale bar, 5 μ m.

D Comparison of cell sensitivity to IR. HeLa cells transfected with indicated siRNA (*N* = 500) were plated and treated with the indicated doses of IR. The number of surviving colonies was counted 14 days after IR treatment. The average of three independent experiments is shown. The error bars indicate the standard deviation.

E Comparison of homologous recombination repair capacity in DR-GFP U2OS cells transfected with the indicated siRNAs. U2OS cells harboring the DR-GFP reporter were treated with the indicated siRNAs, followed by transfection with the I-SCEI expression vector. Two days later, GFP expression was accessed by flow cytometry. BRCA2 depletion was used as a negative control. The GFP expression levels are shown as the average of three independent experiments, and the error bars indicate the standard deviation.

addition, PWWP2B appeared to promote HR by facilitating DNA end resection in response to IR. Notably, the mutation status of PWWP2B showed a strong association with the overall survival duration of gastric cancer patients (Fig 1). In summary, we

demonstrated not only the biological importance of PWWP2B in the IR-induced DDR pathway and HR-mediated DSB repair but also its importance in clinical settings, especially in the prognosis of cancer patients based on its mutational status and mRNA expression level.

Materials and Methods

Subjects

Genomic DNA was obtained from 25 gastric cancer patients after obtaining written informed consent. The Institutional Review Board of Hallym University Sacred Heart Hospital, Anyang-si, South Korea, approved this study (HUSHH IRB No: 2015-1078).

The identification of somatic mutations and driver genes in gastric cancer tissues

Sequencing reads generated from the whole-exome sequencing of 25 stomach adenocarcinoma (STAD) patients' samples were aligned to the GRCh37 human reference genome using BWA-MEM (ver. 0.7.15) with the “-M” option (preprint: Li, 2013). The mapped BAM files were sorted and indexed using samtools (ver. 1.6; Li et al, 2009). Duplicate reads were removed using Picard (ver.2.9.0) with the MarkDuplicates module (<http://broadinstitute.github.io/picard>). The mapping quality was recalibrated using the BaseRecalibrator and the PrintReads modules using the Genome Analysis Tool Kit (GATK) (ver. 3.7; DePristo et al, 2011). Somatic single-nucleotide variants (SNVs) and indels were identified using MuTect2 (Cibulskis et al, 2013) in the GATK (ver 4.1.0.0) with the “--disable-read-filter MateOnSameContigOrNoMappedMateReadFilter” and “--max-mnp-distance 0” options. All variants identified by MuTect2 were filtered using the FilterMutectCalls module with default options and annotated using the Ensembl Variants Effect Predictor (ver. 92.1; McLaren et al, 2016). Mutations in three tumor samples without matched normal samples were filtered using the “--panel-of-normals” option when running MuTect2. The panel of normals was generated using the CreateSomaticPanelOfNormals module in GATK based on 22 tissue and blood normal samples. We further applied the 1000 Genome Project and a gnomAD-based allele frequency cutoff ($AF < 0.001$) for the three samples without matched normal samples to filter out potential germline variants. For driver gene detection, we used the MutSigCV (ver 1.41; Lawrence et al, 2013) algorithm with default options. The potential impact of mutations in protein sequences was predicted by SIFT (Ng & Henikoff, 2003), PolyPhen (Adzhubei et al, 2010), and SNPEff (Cingolani et al, 2012).

GST pull-down

Glutathione S-transferase (GST) fusion protein or GST was expressed in *Escherichia coli* and immobilized on glutathione-Sepharose 4B beads. The cell lysates of the HEK293T cells transfected with plasmids encoding the indicated proteins were incubated with the GST fusion protein or GST for 1 h at 4°C. After washing with NETN buffer, the samples were subjected to SDS-PAGE. Western blotting was performed using the antibodies indicated in each figure legend.

Laser microirradiation and imaging of cells

The accumulation of GFP-UHRF1 wild-type or mutants, and GFP-PWWP2B wild-type or mutants was analyzed as previously described (Min et al, 2014).

Homologous recombination and non-homologous end-joining assay

The homologous recombination assay was performed as previously described (Gunn et al, 2011). U2OS DR-GFP or EJ5-GFP cells were first treated with the indicated siRNAs in 24-well plates and then transfected with 0.4 µg of I-SceI per well 24 h after siRNA transfection. Seventy-two hours after I-SceI transfection, the cells were trypsinized, and the percentage of GFP-positive cells was determined by flow cytometry. Statistical analysis was performed by the paired *t*-test. BD FACSCanto II (NFEC-2011-02-145106) is used for FACS analysis at the Core Facility Center for Chronic and Metabolic Diseases at Sookmyung Women's University.

Quantitative analysis of end resection using ER-AsiSI U2OS cells

Quantitative analysis of end resection using ER-AsiSI U2OS cells was performed as previously described (Zhou et al, 2014). ER-AsiSI U2OS cells were grown in Dulbecco's modified Eagle's medium containing 10% FBS. siRNA transfection of ER-AsiSI U2OS cells was performed using Lipofectamine RNAiMAX (Invitrogen) following the manufacturer's instructions. The ER-AsiSI U2OS cells were treated with mock or 4-hydroxytamoxifen (4-OHT, Sigma; H7904) for 4 h. The ER-AsiSI U2OS cells were collected at a concentration of 1.2×10^7 cells/ml with 37°C 0.6% low-gelling point agarose (Bio-Rad) in PBS. A 50 µl cell suspension was dropped on Parafilm (Pechiney) to make a solidified agar ball, then transferred to a tube. The agar ball was treated with 1 ml of ESP buffer (0.5 M EDTA, 2% N-lauroylsarcosine, 1 mg/ml proteinase-K, and 1 mM CaCl₂, pH 8.0) for 20 h at 16°C with rotation, followed by treatment with 1 ml of HS buffer (1.85 M NaCl, 0.15 M KCl, 5 mM MgCl₂, 2 mM EDTA, 4 mM Tris, and 0.5% Triton X-100, pH 7.5) for 20 h at 16°C with rotation. After washing with 1 ml of PBS for 6 h at 4°C with rotation, the agar ball was melted by placing the tube in a 68°C heat block for 10 min. The melted sample was diluted 15-fold with 68°C ddH₂O and mixed with an equal volume of the appropriate restriction enzyme buffer. The resection near the specific DSBs was measured by quantitative polymerase chain reaction (qPCR) analysis. The sequences of the qPCR primers and probes are listed in Appendix Table S2. The genomic DNA sample (36 µl) was digested with 80 units of BsrGI or HindIII (New England Biolabs) restriction enzymes at 37°C overnight. The digested samples (3 µl) were used as templates in a 25-µl qPCR containing 12.5 µl of TaqMan Universal PCR Master Mix (ABI), 0.5 mM of each primer, and 0.2 mM probe using a QuantStudio 7 Flex Real-Time PCR System (ABI). The percentage of ssDNA generated by resection at the selected sites was calculated as previously described (Zhou et al, 2014). For each sample, the Ct was calculated by subtracting the Ct value of the mock-digested sample from the Ct value of the digested sample. The percentage of ssDNA was calculated by the following equation: $ssDNA (\%) = 1/(2^{(4Ct-1)} + 0.5) * 100$.

Statistical analysis

To identify the impact of PWWP2B mutations on disease prognosis, the overall survival (OS) of the two groups categorized by mutational status were compared. Overall survival was defined as the duration from the diagnosis to any cause of death. We used the Kaplan–Meier method and log-rank tests for survival analysis. Additionally, univariate and

multivariate analyzes were performed to adjust for the potential interference of other variables. The multivariate Cox regression model was developed with a backward likelihood ratio by selecting variables that had a *P*-value of < 0.01 in the univariate analysis. Two-sided *P*-values of < 0.05 were considered statistically significant. All statistical analyzes were performed using the Statistical Package for the Social Sciences (IBM SPSS, Chicago, IL, USA) version 21.0.

Data availability

Whole-exome sequencing data have been deposited at <https://www.ncbi.nlm.nih.gov/bioproject/PRJNA673924>. All the materials, methods, and materials presented in this study are available upon request.

Expanded View for this article is available online.

Acknowledgements

We thank the members of Hongtae Kim's laboratory for critical discussions and Jinhui Jeong, a clinical research coordinator, for organizing the clinical research data. This work was supported by the Institute for Basic Science (IBS-R022-D1 to HK and KM), National Research Foundation of Korea (NRF) grants funded by the Korean government (MEST) (NRF-2018R1A2B2003129, NRF-2014M3C9A2064688, NRF-2021R1A6A1A03038890, and NRF-2019R1A2C2089746), the National R&D Program for Cancer Control, Ministry of Health and Welfare (HA17C0054 to DYZ), and the Hallym University Research Fund to DYZ. Funding for open access charge: IBS-R022-D1 to HK and KM.

Author contributions

Min Kyung Ju: Investigation. **Joo Rack Lee:** Investigation. **Yeonsong Choi:** Investigation. **Seon Young Park:** Investigation. **Hee Jung Sul:** Investigation. **Hee Jin Chung:** Investigation. **Soyeong An:** Investigation. **Semin Lee:** Investigation. **Eunyoung Jung:** Investigation. **Bohyun Kim:** Data curation. **Bo-Youn Choi:** Data curation. **Bum Jun Kim:** Data curation. **Hyeong Su Kim:** Data curation. **Hyun Lim:** Data curation. **Ho Suk Kang:** Data curation. **Jae Seung Soh:** Data curation. **Kyungjae Myung:** Investigation. **Kab Choong Kim:** Data curation. **Ji Woong Cho:** Data curation. **Jinwon Seo:** Data curation. **Tae Moon Kim:** Investigation. **Ja Yil Lee:** Investigation. **Yonghwan Kim:** Conceptualization; Data curation; Funding acquisition; Investigation; Writing - original draft; Writing - review & editing. **Hongtae Kim:** Conceptualization. **Dae Young Zang:** Conceptualization.

In addition to the CRediT author contributions listed above, the contributions in detail are:

KM, YK, HK, and DYZ designed the experiment. MKJ, JRL, SL, SYP, HJS, HJC, TMK, and YC conducted the experiment. HJS, BK, BYC, BJK, HSKi, HL, HSKa, JSS, KCK, SA, JYL, EJ, JWC, and JS collected and prepared the clinical samples and analyzed the clinical data. HK, YK, and DYZ supervised the project and wrote the manuscript with input from MKJ, JRL, SL, TMK, and BJK.

Disclosure and competing interests statement

The authors declare that they have no conflict of interest.

References

Adzhubei IA, Schmidt S, Peshkin L, Ramensky VE, Gerasimova A, Bork P, Kondrashov AS, Sunyaev SR (2010) A method and server for predicting damaging missense mutations. *Nat Methods* 7: 248–249

- Alves IT, Cano D, Böttcher R, van der Korput H, Dinjens W, Jenster G, Trapman J (2017) A mononucleotide repeat in PRRT2 is an important, frequent target of mismatch repair deficiency in cancer. *Oncotarget* 8: 6043
- An CH, Je EM, Yoo NJ, Lee SH (2015) Frameshift mutations of cadherin genes DCHS2, CDH10 and CDH24 genes in gastric and colorectal cancers with high microsatellite instability. *Pathol Oncol Res* 21: 181–185
- Aparicio T, Baer R, Gautier J (2014) DNA double-strand break repair pathway choice and cancer. *DNA Repair* 19: 169–175
- Aymard F, Bugler B, Schmidt CK, Guillou E, Caron P, Brioso S, Iacovoni JS, Daburon V, Miller KM, Jackson SP et al (2014) Transcriptionally active chromatin recruits homologous recombination at DNA double-strand breaks. *Nat Struct Mol Biol* 21: 366–374
- Cancer Genome Atlas Research Network (2014) Comprehensive molecular characterization of gastric adenocarcinoma. *Nature* 513: 202
- Cerami E, Gao J, Dogrusoz U, Gross BE, Sumer SO, Aksoy BA, Jacobsen A, Byrne CJ, Heuer ML, Larsson E (2012) The cBio cancer genomics portal: an open platform for exploring multidimensional cancer genomics data. *Cancer Discov* 2: 401–404
- Cibulskis K, Lawrence MS, Carter SL, Sivachenko A, Jaffe D, Sougnez C, Gabriel S, Meyerson M, Lander ES, Getz G (2013) Sensitive detection of somatic point mutations in impure and heterogeneous cancer samples. *Nat Biotechnol* 31: 213
- Cingolani P, Platts A, Le Wang L, Coon M, Nguyen T, Wang L, Land SJ, Lu X, Ruden DM (2012) A program for annotating and predicting the effects of single nucleotide polymorphisms, SnpEff: SNPs in the genome of *Drosophila melanogaster* strain w1118; iso-2; iso-3. *Fly* 6: 80–92
- Cortes-Ciriano I, Lee S, Park W-Y, Kim T-M, Park PJ (2017) A molecular portrait of microsatellite instability across multiple cancers. *Nat Commun* 8: 15180
- Cruz-García A, Lopez-Saavedra A, Huertas P (2014) BRCA1 accelerates CtIP-mediated DNA-end resection. *Cell Rep* 9: 451–459
- Daugaard M, Baude A, Fugger K, Povlsen LK, Beck H, Sørensen CS, Petersen NHT, Sorensen PHB, Lukas C, Bartek J et al (2012) LEDGF (p75) promotes DNA-end resection and homologous recombination. *Nat Struct Mol Biol* 19: 803
- DePristo MA, Banks E, Poplin R, Garimella KV, Maguire JR, Hartl C, Philippakis AA, del Angel G, Rivas MA, Hanna M et al (2011) A framework for variation discovery and genotyping using next-generation DNA sequencing data. *Nat Genet* 43: 491
- Eidahl JO, Crowe BL, North JA, McKee CJ, Shkriabai N, Feng L, Plumb M, Graham RL, Gorelick RJ, Hess S et al (2013) Structural basis for high-affinity binding of LEDGF PWWP to mononucleosomes. *Nucleic Acids Res* 41: 3924–3936
- Falchetti M, Saieva C, Lupi R, Masala G, Rizzolo P, Zanna I, Ceccarelli K, Sera F, Mariani-Costantini R, Nesi G et al (2008) Gastric cancer with high-level microsatellite instability: target gene mutations, clinicopathologic features, and long-term survival. *Hum Pathol* 39: 925–932
- Fitzmaurice C, Allen C, Barber RM, Barregard L, Bhutta ZA, Brenner H, Dicker DJ, Chimed-Orchir O, Dandona R, Dandona L et al (2017) Global, regional, and national cancer incidence, mortality, years of life lost, years lived with disability, and disability-adjusted life-years for 32 cancer groups, 1990 to 2015: a systematic analysis for the global burden of disease study. *JAMA Oncol* 3: 524–548
- Giannakis M, Mu X, Shukla S, Qian Z, Cohen O, Nishihara R, Bahl S, Cao Y, Amin-Mansour A, Yamauchi M et al (2016) Genomic correlates of immune-cell infiltrates in colorectal carcinoma. *Cell Rep* 15: 857–865

- Goldberg M, Stucki M, Falck J, D'Amours D, Rahman D, Pappin D, Bartek J, Jackson SP (2003) MDC1 is required for the intra-S-phase DNA damage checkpoint. *Nature* 421: 952–956
- Gunn A, Bennardo N, Cheng A, Stark JM (2011) Correct end use during end joining of multiple chromosomal double strand breaks is influenced by repair protein RAD50, DNA-dependent protein kinase DNA-PKs, and transcription context. *J Biol Chem* 286: 42470–42482
- Haron NH, Hanif EAM, Abdul MR, Manaf JAY, Harun R, Mohamed R, Mohamed I (2019) Microsatellite instability and altered expressions of MLH1 and MSH2 in gastric cancer. *Asian Pac J Cancer Prev* 20: 509–517
- Harper JW, Elledge SJ (2007) The DNA damage response: ten years after. *Mol Cell* 28: 739–745
- Hiyama T, Tanaka S, Yoshihara M, Sasao S, Kose K, Shima H, Tuncel H, Ueno Y, Ito M, Kitadai Y et al (2004) Chromosomal and microsatellite instability in sporadic gastric cancer. *J Gastroenterol Hepatol* 19: 756–760
- Karimi P, Islami F, Anandasabapathy S, Freedman ND, Kamangar F (2014) Gastric cancer: descriptive epidemiology, risk factors, screening, and prevention. *Cancer Epidemiol Biomarkers Prev* 23: 700–713
- Kondratova A, Watanabe T, Marotta M, Cannon M, Segall AM, Serre D, Tanaka H (2015) Replication fork integrity and intra-S phase checkpoint suppress gene amplification. *Nucleic Acids Res* 43: 2678–2690
- Lawrence MS, Stojanov P, Polak P, Kryukov GV, Cibulskis K, Sivachenko A, Carter SL, Stewart C, Mermel CH, Roberts SA et al (2013) Mutational heterogeneity in cancer and the search for new cancer-associated genes. *Nature* 499: 214
- Lee JH, Paull TT (2004) Direct activation of the ATM protein kinase by the Mre11/Rad50/Nbs1 complex. *Science* 304: 93–96
- Li H (2013) Aligning sequence reads, clone sequences and assembly contigs with BWA-MEM. *arXiv* <https://doi.org/10.48550/arXiv.1303.3997> [PREPRINT]
- Li H, Handsaker B, Wysoker A, Fennell T, Ruan J, Homer N, Marth G, Abecasis G, Durbin R (2009) The sequence alignment/map format and SAMtools. *Bioinformatics* 25: 2078–2079
- Li Z, Li J, Kong Y, Yan S, Ahmad N, Liu X (2017) Plk1 phosphorylation of Mre11 antagonizes the DNA damage response. *Cancer Res* 77: 3169–3180
- Liang C-C, Zhan B, Yoshikawa Y, Haas W, Gygi SP, Cohn MA (2015) UHRF1 is a sensor for DNA interstrand crosslinks and recruits FANCD2 to initiate the Fanconi anemia pathway. *Cell Rep* 10: 1947–1956
- Maurer-Stroh S, Dickens NJ, Hughes-Davies L, Kouzarides T, Eisenhaber F, Ponting CP (2003) The Tudor domain 'Royal Family': tudor, plant agenet, chromo, PWWP and MBT domains. *Trends Biochem Sci* 28: 69–74
- McLaren W, Gil L, Hunt SE, Riat HS, Ritchie GR, Thormann A, Flicek P, Cunningham F (2016) The ensembl variant effect predictor. *Genome Biol* 17: 122
- Mills KD, Ferguson DO, Alt FW (2003) The role of DNA breaks in genomic instability and tumorigenesis. *Immunol Rev* 194: 77–95
- Min S, Jo S, Lee HS, Chae S, Lee JS, Ji JH, Cho H (2014) ATM-dependent chromatin remodeler Rsf-1 facilitates DNA damage checkpoints and homologous recombination repair. *Cell Cycle* 13: 666–677
- Ng PC, Henikoff S (2003) SIFT: predicting amino acid changes that affect protein function. *Nucleic Acids Res* 31: 3812–3814
- van Nuland R, van Schaik FM, Simonis M, van Heesch S, Cuppen E, Boelens R, Timmers HM, van Ingen H (2013) Nucleosomal DNA binding drives the recognition of H3K36-methylated nucleosomes by the PSIP1-PWWP domain. *Epigenetics Chromatin* 6: 12
- Ouyang H, Furukawa T, Abe T, Kato Y, Horii A (1998) The BAX gene, the promoter of apoptosis, is mutated in genetically unstable cancers of the colorectum, stomach, and endometrium. *Clin Cancer Res* 4: 1071–1074
- Pfister S, Ahrabi S, Zalmas L-P, Sarkar S, Aymard F, Bachrati CZ, Helleday T, Legube G, La Thangue N, Porter A et al (2014) SETD2-dependent histone H3K36 trimethylation is required for homologous recombination repair and genome stability. *Cell Rep* 7: 2006–2018
- Qin S, Min J (2014) Structure and function of the nucleosome-binding PWWP domain. *Trends Biochem Sci* 39: 536–547
- Qiu C, Sawada K, Zhang X, Cheng X (2002) The PWWP domain of mammalian DNA methyltransferase Dnmt3b defines a new family of DNA-binding folds. *Nat Struct Mol Biol* 9: 217
- Qiu YU, Zhang W, Zhao C, Wang Y, Wang W, Zhang J, Zhang Z, Li G, Shi Y, Tu X et al (2012) Solution structure of the Pdp1 PWWP domain reveals its unique binding sites for methylated H4K20 and DNA. *Biochem J* 442: 527–538
- Sartori AA, Lukas C, Coates J, Mistrik M, Fu S, Bartek J, Baer R, Lukas J, Jackson SP (2007) Human CtIP promotes DNA end resection. *Nature* 450: 509–514
- Scully R, Panday A, Elango R, Willis NA (2019) DNA double-strand break repair-pathway choice in somatic mammalian cells. *Nat Rev Mol Cell Biol* 20: 698–714
- Soo Lee N, Jin Chung H, Kim H-J, Yun Lee S, Ji J-H, Seo Y, Hun Han S, Choi M, Yun M, Lee S-G et al (2016) TRAP1/RNF206 is required for recruitment of RAP80 to sites of DNA damage. *Nat Commun* 7: 10463
- Stiff T, O'Driscoll M, Rief N, Iwabuchi K, Lobrich M, Jeggo PA (2004) ATM and DNA-PK function redundantly to phosphorylate H2AX after exposure to ionizing radiation. *Cancer Res* 64: 2390–2396
- Tian Y, Paramasivam M, Ghosal G, Chen D, Shen XI, Huang Y, Akhter S, Legerski R, Chen J, Seidman M et al (2015) UHRF1 contributes to DNA damage repair as a lesion recognition factor and nuclease scaffold. *Cell Rep* 10: 1957–1966
- Wang Z, Gong Y, Peng B, Shi R, Fan D, Zhao H, Zhu M, Zhang H, Lou Z, Zhou J et al (2019) MRE11 UFMylation promotes ATM activation. *Nucleic Acids Res* 47: 4124–4135
- Zhang H, Liu H, Chen Y, Yang XU, Wang P, Liu T, Deng M, Qin BO, Correia C, Lee S et al (2016) A cell cycle-dependent BRCA1-UHRF1 cascade regulates DNA double-strand break repair pathway choice. *Nat Commun* 7: 10201
- Zhang T, Wei G, Millard CJ, Fischer R, Konietzny R, Kessler BM, Schwabe JW, Brockdorff N (2018) A variant NuRD complex containing PWWP2A/B excludes MBD2/3 to regulate transcription at active genes. *Nat Commun* 9: 3798
- Zhou Y, Caron P, Legube G, Paull TT (2014) Quantitation of DNA double-strand break resection intermediates in human cells. *Nucleic Acids Res* 42: e19